Evidence that the 127–164 Region of Prion Proteins Has Two Equi-Energetic Conformations with β or α Features

Philippe Derreumaux
Information Génétique et Structurale, CNRS-UMR 1889, 13402 Marseille, France

ABSTRACT Prion proteins cause neurodegenerative illnesses in humans and animals. The diseases are associated with a topological change from a predominantly α (PrP^C) to β-sheet (PrP^{Sc}) structure. Many studies have focused on the minimum sequence requirements and key events for developing or transmitting disease. Here, we report on the application of molecular modeling studies to predict the lowest-energy conformations for five fragments in solution at pH 7. We show that PrP(143–158) adopts a helix, the model PrP(106–126), PrP(142–167), and PrP(143–178) peptides have a clear preference for a variety of β-sheet structures, whereas PrP(127–164) has two iso-energetic conformations with all β or $\alpha\beta$ native-like structures. Such a finding for PrP(127–164), which explains a large body of experimental data, including the location of all mutations causing prion diseases, may have important implications for triggering or propagating the topological change.

INTRODUCTION

Prion proteins are intriguing biopolymers because they can act as infectious agents by causing self-propagating conformational changes (Sparrer et al., 2000). They are also distinct from other proteins because, at present, 24 mutations distributed throughout their sequences (see below) lead to disorders, including Creutzfeld-Jacob disease (CJD) and Gerstmann-Straussler-Scheinker (GSS) disease in humans, scrapie in sheep, and bovine spongiform encephalopathy in cows. Within the protein-only hypothesis, a detailed mechanism for the conformational transition is still unclear, although two models have been proposed. The template-assisted model suggests that the transition from monomeric α-helical PrP^C to monomeric β-rich PrP^{Sc} is the rate-limiting step, followed by fast oligomerization of the subunits (Huang et al., 1996). Alternatively, the nucleation-polymerization and β-nucleation models propose that molecular association facilitates a conformational change in the monomer and that aggregation of a PrP^{Sc} nucleus of critical size is the rate-limiting step (Jarrett and Lansbury, 1993; Morrisey and Shakhnovich, 1999).

The physiological monomeric PrP^C structure for murine (m), Syrian hamster, and human (hu) sequences has been characterized by NMR spectroscopy as adopting an unstructured region from residues 1 to 121 and a globular domain with a two-stranded anti-parallel β-sheet and three α-helices (Riek et al., 1996; Zahn et al., 2000). The β-strands S1 and S2 comprise residues 128–131 and 161–164, respectively. The first helix, labeled H1, spans residues 144–153. The helices H2 (from residues 172 to 194) and H3 (from residues 200 to 224) are bridged by a disulfide bond (Cys179–Cys214) and make several contacts with H1, S1, and S2 (Fig. 1).

The scrapie multimeric structure, PrP^{Sc}, has not been characterized experimentally but is known to have less α-helix and more β-sheet content than PrP^C. Three hypothetical structural models for PrP^{Sc} have been proposed based on immunological studies and circular dichroism (CD) spectra. In the first model, the region between residues 90 and 145 was modeled by two consecutive β-hairpins (four strands) with strand 1 parallel to strand 3 (Huang et al., 1996). In the second model, the secondary H1, S1, and S2 structural elements have been replaced by four adjacent anti-parallel β-strands that form a Greek key motif (Korth et al., 1997). In the last model, PrP^{Sc} adopts β-helical conformations (Downing and Lazo, 1999).

The availability of truncated prion proteins has provided new insights into the minimum sequence requirements for prion propagation. The N-terminally truncated PrP at residue 90, PrP(90–231) also termed PrP 27–30 (Prusiner, 1997), and the C-terminally truncated PrP at residue 145 (Ghetti et al., 1996) are disease causing, indicating that the PrP(90–145) fragment is the minimal infectious unit. Recent studies have also shown that PrP106, which includes residues 89–140 and 177–230 of full-length PrP with the intact disulfide bond, i.e., removes the region in PrP^C that form H1 and S_2, also retains the ability to support PrP^{Sc} formation in transgenic mice (Supatapone et al., 1999). However, because PrP106 is unstructured at low concentrations (Baskakov et al., 2000), PrP(90–145) is random coil in monomeric form (Zhang et al., 1995), and the NMR solution structure of PrP(90–231) is superposable on the full sequence structure (James et al., 1997), only the 90–231 region provides opportunities for understanding the topological change.

The aim of this study is to determine whether certain fragments encompassing the 106–178 region have distinct conformational properties in equilibrium at pH 7 and therefore could trigger the conformational change in PrP^C. There

Received for publication 31 January 2001 and in final form 14 May 2001.
Address reprint requests to Dr. Philippe Derreumaux, Information Génétique et Structurale, CNRS-UMR 1889, 31 Chemin Joseph Aiguier, 13402 Marseille, France. Tel.: 33-4-91164603; Fax: 33-4-91164549; E-mail: philippe@igs.cnrs-mrs.fr.

0006-3495/01/09/1657/09 $2.00

A

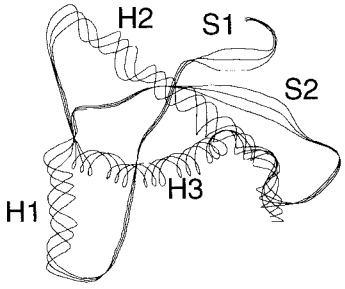

B

Structure	S1	H1	S2	H2
huPrP(127-178)	GYMLGSAMSRPIIHFGSDYEDRYYRENMHRYPNQVYYRPMDEYSNQNNFVHD			
mPrP(143-158)	NDWEDRYYRENMYRYP			
mPrP(142-167)	GNDWEDRYYRENMYRYPNQVYYRPVC			
huPrP(143-178)	SDYEDRYYRENMHRYPNQVYYRPMDEYSNQNNFVHD			
huPrP(127-164)	GYMLGSAMSRPIIHFGSDYEDRYYRENMHRYPNQVYYR			
huPrP(106-126)	KTNMKHMAGAAAAGAVVGGLG			
chPrP(127-164)	GYAMGRVMSGMNYHFDSPDEYRWWSENSARYPNRVYYR			
1f71(101-138)	SAAELRHVMTNLGEKLTDEEVDEMIREADIDGDGQVNY			
1lyd(30-67)	GHLLTKSPSLNAAKSELDKAIGRNCNGCITKDEAEKLF			
T41118(47-84)	GYCLNSNCSKPLVGYNSDYLDEHAKDGFRTSVIVRQRA			
1mil0(40-77)	QYVLTGLQSGQPKHLLLVDPEGVVRTKDHRFESVSHLI			

FIGURE 1 (*A*) NMR structure of PrP(121–231) from mouse, PDB entry 1AG2 (Riek et al., 1996). The helices H1, H2, and H3 and the β-strands S1 and S2 are shown. (*B*) Sequences of the five PrP peptides, which are the subject of OPEP-MC prediction, and sequences of the five control peptides (see text). The residues involved in the β-strands S1 and S2 and in helices H1 and H2 within the NMR protein structure are underlined. Abbreviations for the amino acids are as follows: A, Ala; C, Cys; D, Asp; E, Glu; F, Phe; G, Gly; H, His; I, Ile; K, Lys; L, Leu; M, Met; N, Asn; P, Pro; Q, Gln; R, Arg; S, Ser; V, Val; W, Trp; Y, Tyr.

is experimental evidence that such transition occurs under acidic conditions (Hornemann and Glockshuber, 1998). Despite its conformational change during conversion of PrP^{C} into PrP^{Sc} (Peretz et al., 1997), the region comprising residues 90–105 is not taken into account because it is a highly disordered fragment, as determined by NMR spectroscopy (James et al., 1997). The 179–231 region is also excluded because the disulfide bridge within the two-helix bundle is required for PrP^{Sc} formation (Prusiner, 1997) and the PrP structure with reduced disulfide bridge is characterized by a major loss of α-helix and increased proportion of an unordered structure (Maiti and Surewicz, 2000).

Ideally, one would like to simulate the all-atom 106–178 fragment folding process by molecular dynamics simulations. However, the computation time for one 1-ms trajectory is not tractable yet, although recent progress has been reported (Duan and Kollman, 1998). As an alternative, we use a simple model of protein folding that allows extensive sampling of conformational space. The Monte Carlo (MC)-based approach searches the lowest-energy conformation for the target sequence by global optimization of an effective potential (OPEP) starting from randomly chosen or fully extended conformations (Derreumaux, 1999). Such simulations were found to reproduce the topological features for 31 peptides in aqueous solution, including two- and three-helix bundles, all β (β_3) and mixed α/β ($\beta_2\alpha$, $\beta\alpha\beta$) motifs (Derreumaux, 2000).

In this work, we apply the OPEP-MC approach to predict the lowest-energy conformations for five polypeptides. The sequences are given in Fig. 1. The energies of these conformations are also calculated using two independent physical all-atom energy models (see Materials and Methods).

The first three peptides have been extensively characterized by NMR and/or CD spectroscopy and thus allow direct comparison between generated and experimental averages in aqueous solution. Such a test is not easy because the fragment mPrP(143–158), which in PrP^{C} forms helix H1, shows helical preferences (Liu et al., 1999), but mPrP(142–167), which in PrP^{C} forms H1 and the β-strand S2, shows strong β-hairpin conformational preferences (S. Kozin and P. Debey, in preparation), whereas the fragment huPrP(106–126) samples various secondary structures when characterized under different conditions (Salmona et al., 1999). The latter peptide was also chosen because it exhibits some of the pathogenic and physicochemical properties of PrP^{Sc} (Brown et al., 1996), is cytotoxic in vivo (Ettaiche et al., 2000), and is adjacent to the 127–164 segment.

The last two model huPrP(127–164) and huPrP(143–178) peptides have not been studied experimentally but extend mPrP(142–167) at both extremities and help clarify the stability of the β-hairpin structure in different environments. Furthermore, huPrP(127–164) includes H1 and the β-strands S1 and S2.

MATERIALS AND METHODS

The OPEP-MC protocol simplifies both geometry and energy representations (Derreumaux, 1999, 2000). It uses a flexible-geometry model where each amino acid is represented by six particles, i.e., N, H, Cα, C, O, and one bead with an appropriate van der Waals radius and position for the side chains. All bond lengths, bond angles, and backbone dihedral angles ϕ, ψ are free to vary except the peptide bond dihedral angles ω, which are fixed at 180°. This representation reproduces experimental structures and backbone hydrogen bonds exactly. This is not always possible in other simplified or lattice-based schemes.

The polypeptide energy surface is modeled by a knowledge-based potential, including solvent effects. The analytic form was obtained by maximizing the stability gap between the energy of the native structure and a representative ensemble of non-native structures for four training peptides with 10–28 residues (Derreumaux, 1999). The final potential optimizes the balance between short-range and long-range (along the sequence) interactions and includes weighted (w) contributions from hydrogen bonds (E_{HB}), bond lengths and bond angles (E_{L}), pairwise interactions between side chains (SCs) and α-carbons ($C\alpha$), and finally, α-helix, β-strand, and α_{L} conformational propensities for the 20 amino acids:

$$E = w_{\mathrm{H}}E_{\mathrm{HB1}} + w_{\mathrm{HH}}E_{\mathrm{HB2}} + w_{\mathrm{L}}E_{\mathrm{L}} + w_{\mathrm{SC}}E_{\mathrm{SC,SC}} + w_{\mathrm{A}}E_{\mathrm{C\alpha,C\alpha}} + \sum_{20} w_{\mathrm{P}}^{\alpha}E_{\mathrm{P}}^{\alpha} + \sum_{20} w_{\mathrm{p}}^{\beta}E_{\mathrm{P}}^{\beta} + \sum_{20} w_{\mathrm{P}}^{\alpha_{\mathrm{L}}}E_{\mathrm{P}}^{\alpha_{\mathrm{L}}} \quad (1)$$

The motion of the polypeptide chain is simulated with a diffusion-process-controlled MC approach. This approach does not impose a predefined set of conformational moves. Rather, the next conformation is generated by diffusion-process-controlled moves, which limit the transition time from the current conformation, is then minimized using the conjugate gradient method, and subsequently accepted or rejected by the Metropolis criterion based on some function of the energy change between the current and the next conformations (Metropolis et al., 1953).

For each peptide, eight simulations were performed for 12,000 MC steps starting from fully extended or randomly chosen compact conformations. The temperature T is set to 700 K to accelerate conformational sampling. Three additional runs at 400 K were also carried out on PrP(106–126) and PrP(142–167) for 20,000 MC steps. Consistency between the runs for different starting conformations and different temperatures and the fact that the peptides revisit the same conformational ensemble in the range 10,000–20,000 MC steps probably indicate that most globally optimal (the lowest-energy) conformations have been located. One simulation on hPrP(143–178) and hPrP(127–164) was also carried out at 400 K during 500 MC steps from their conformations within the protein structure to seek their lowest-energy conformations using OPEP. These conformations, which are the subject of energy minimization, are referred to as NMR-minimized conformations.

Because uncertainties in the OPEP energy model cannot be totally excluded, two independent physical all-atom potentials are also used to estimate the energy of the final OPEP-MC-generated conformations. The first energy model is EEF1, which combines the CHARMM19 polar hydrogen potential energy function and a simple Gaussian model for the solvation free energy (Lazaridis and Karplus, 1998). This potential was found to provide a realistic picture of the effective energy surface for a number of test proteins. The second representation is the AMBER molecular mechanics function with a generalized Born solvent model, referred to as AMBERGB (Case et al., 1999). Both potentials were used as recommended by their authors (http://mingus.sci.ccny.cuny.edu/and http://www.amber.ucsf.edu/amber/). Because the side chains of all amino acids are represented by one bead, the all-atom models were generated using the MaxSprout program (Holm and Sander, 1992) and the based mean-field Confmat algorithm (Koehl and Delarue, 1994). These two sets of conformations for each peptide allow one to examine the effect of different side-chain packings on the total energy.

RESULTS

Accurate prediction for PrP(143–158), PrP(142–167), and PrP(106–126)

As a first step toward understanding the topological change in prion proteins, we verify that the OPEP-MC protocol generates conformational distributions for mPrP(143–158), mPrP(142–167), and huPrP(106–126) in agreement with CD or NMR spectroscopy.

The NMR conformational analysis has shown that mPrP(143–158) exists as a mixture of α-helix from residues 144 to 151 (population of 40%) and random coil conformations (60%) in aqueous solution at pH 4.5, suggesting that helix H1 could be preserved during the conformational transition from PrP^{C} to PrP^{Sc} (Liu et al., 1999). This sequence is predicted by OPEP-MC to adopt a helix from residues 146 to 155 and a β-hairpin conformation, which is destabilized by 1.5 $k_{\mathrm{B}}T$ (0.9 kcal/mol) relative to the helical conformation. Such a marginal stability of the dominant conformation has already been noted for other isolated protein fragments.

In Fig. 2, we show the generated ensemble for mPrP (142–167) in aqueous solution. All simulations converge to the vicinity of two distinct topologies. The first fold explored contains either a regular β-hairpin structure with hydrogen-bonding interactions between the strands or a β-hairpin structure without β-sheet hydrogen-bonding interactions. The latter structure is more consistent with NMR spectroscopy at pH 6.5 (S. Kozin and P. Debey, in preparation). In both structures, the turn encompasses residues Glu152 and Tyr155. The energies of these two conformations and the NMR-minimized conformation are identical within $k_{\mathrm{B}}T$. The second fold sampled is of $\beta\alpha\beta$ type with residues Glu152 to Arg156 helical, and residues Trp145, Glu146 and Tyr163, Arg164 forming a two-stranded parallel β-sheet. This $\beta\alpha\beta$ conformation is less stable than the β-hairpin conformations by 4 $k_{\mathrm{B}}T$ and 2.5 $k_{\mathrm{B}}T$ using OPEP and EEF1 (Lazaridis and Karplus, 1998) force fields, respectively. Our ensemble of conformations with extended β and helical structures is interesting because it can reconcile the apparent conflicting NMR data between mPrP(142–167) at pH 6.5 and mPrP(142–170) at pH 3, where H1 remains stable (Sharman et al., 1998). Such a large variation in NMR results can be explained if the peptide undergoes a conformational transition between pH 3 and 6.5. Although sec-

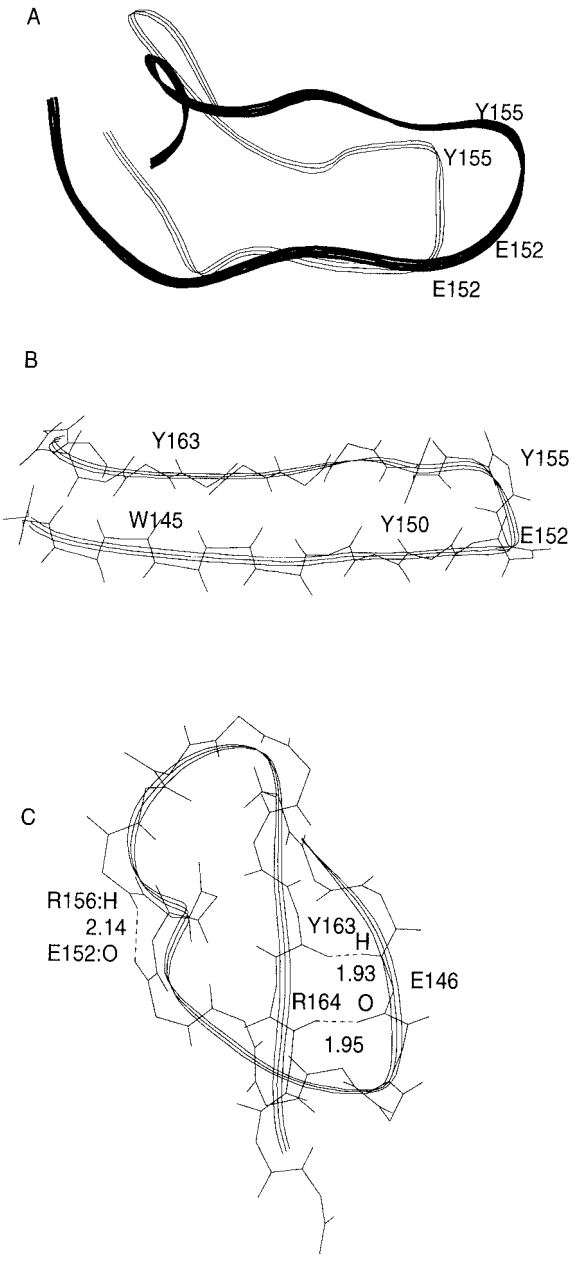

FIGURE 2 The predicted main-chain conformations for mPrP(142–167). Bold, the native NMR structure; gray (*top* and *middle*), the lowest energy structures; gray (*bottom*), the $\beta\alpha\beta$ structure.

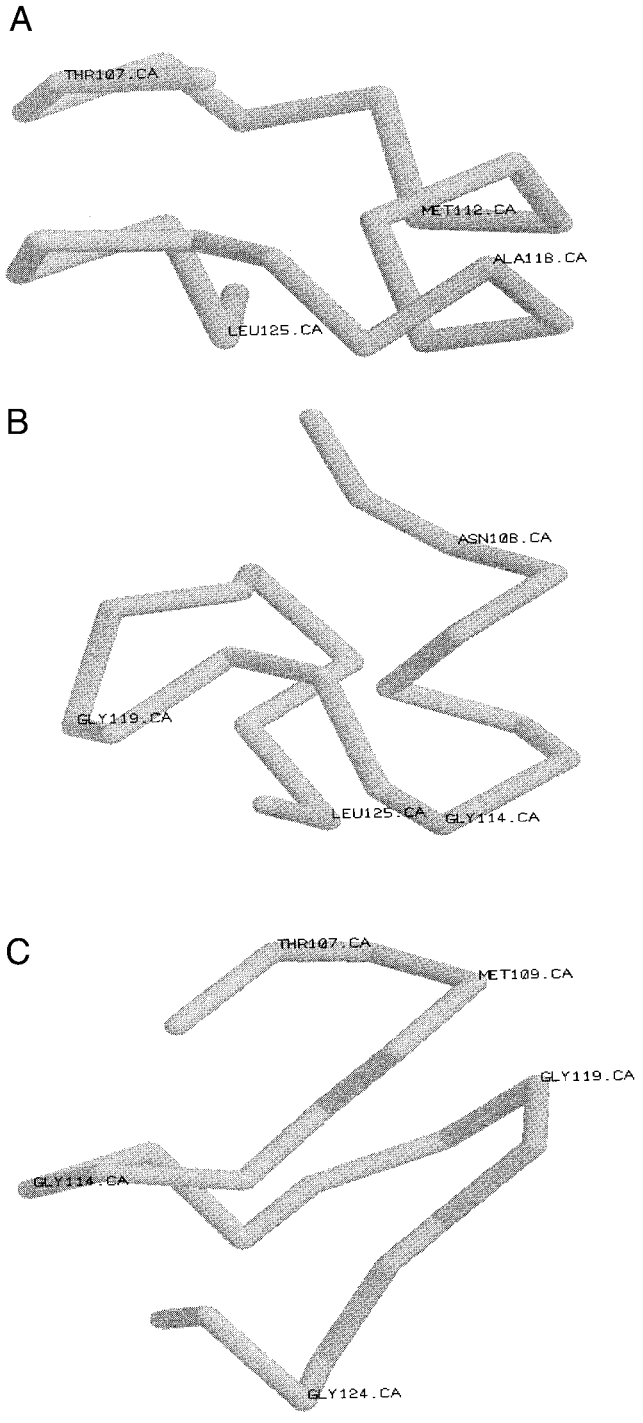

FIGURE 3 The predicted main-chain conformations for huPrP(106–126). The P1 (*A*), P2 (*B*), and P3 (*C*) conformations are shown.

ondary structure of huPrP(106–126) as deduced by CD spectroscopy varies with environmental conditions, PrP(106–126) has a high propensity to form stable β-sheet structures and to assemble into amyloid fibrils (Salmona et al., 1999). PrP(106–126) was characterized as adopting random coil conformation in deionized water and a mixture of α-helix (17%), β-sheet (40%), and random coil (40%) in phosphate buffer at pH 7.0 (Salmona et al., 1999). In contrast to the OPEP-MC simulations on PrP(143–158) and PrP(142–167), the simulations on PrP(106–126) do not always converge to well ordered secondary structures. Fig. 3 shows the three lowest-energy conformations, separated by 4 k_BT using OPEP. The two conformations in Fig. 3, *A* and *B* (P1 and P2) are helical from residues 112 to 118 in P1 and 108 to 113 in P2 with random coil segments, whereas the conformation in Fig. 3 *C* (P3) has three-stranded anti-

parallel β-sheet structural features. The EEF1 results indicate that a rather small energy difference is involved between P1 (−522.9 kcal/mol) and P3 (−521.0 kcal/mol), but P2 is largely destabilized (−509.0 kcal/mol). Such a conformational distribution, without considering entropic effects, agrees qualitatively with CD measurements.

Impact of different environments on the 144–164 region

The predicted structure ensemble for huPrP(127–164) is shown in Fig. 4. It is interesting to note that, once the helix H1 is partially formed in the unfolded states, the simulations will find structures with helical properties. Three runs generate models (M1) that deviate little from the structure within the protein (Fig. 4 *A*). The helix H1 is extended by three residues, the two-stranded anti-parallel β-sheet is less regular (one hydrogen-bonding interaction between N-Gly131 and O-Tyr162 versus two interactions from N-Met129 to O-Tyr163 and N-Gly131 to O-Val161 within the protein structure), but the topology is conserved. Three other runs end up as a more distorted native structure (M2). This structure still contains the helix H1, but the conformation of the two terminal regions has shifted from a two-stranded anti-parallel β-sheet to a parallel β-sheet (Fig. 4 *B*). The last two runs converge to a β_3 structure (M3) consisting of two consecutive β-hairpins (Fig. 4 *C*). The lengths of the β-strands are from Tyr128 to Arg136, Phe141 to Tyr150, and Tyr155 to Tyr163. Thus, the structure of the region comprising residues 144–164 has slightly moved from the NMR solution structure of mPrP(142–167). The turn encompasses residues Tyr150 and Met154 versus Glu152 and Tyr155 in mPrP(142–167). The energies of M1, M2, and M3 are almost identical independently of the force field used. They are within 6 k_BT using OPEP and 13 k_BT using EEF1 (M3, 0; M2, 2; and M1, 8 kcal/mol). The AMBERGB force field (Case et al., 1999) cannot distinguish M1 and M3 (0 kcal/mol) but makes the NMR-minimized conformation very unstable (32 kcal/mol).

The representative predicted structure ensemble for huPrP(143–178) is shown in Fig. 5. We see that the eight simulations point to two β topologies. B1 has a four-stranded β-sheet topology with the β-strand 1 anti-parallel to the β-strand 4 and the region from Ser143 to Tyr162 adopting a β-hairpin structure superposable on the NMR and predicted conformations for mPrP(142–167). B2 has a three-stranded anti-parallel β-sheet topology. The β-strands are from Tyr150 to Tyr156, Tyr162 to Tyr169, and Asn173 to Asp178, indicating a different hydrogen-bonding network in the 142–167 region from that in B1. B1 and B2 differ by an energy of 3 k_BT using OPEP, but B2 is found less stable than B1 by 9 and 35 kcal/mol using EEF1 and AMBERGB, respectively. The NMR-minimized conformation is destabilized by 30 kcal/mol relative to B1 using EEF1.

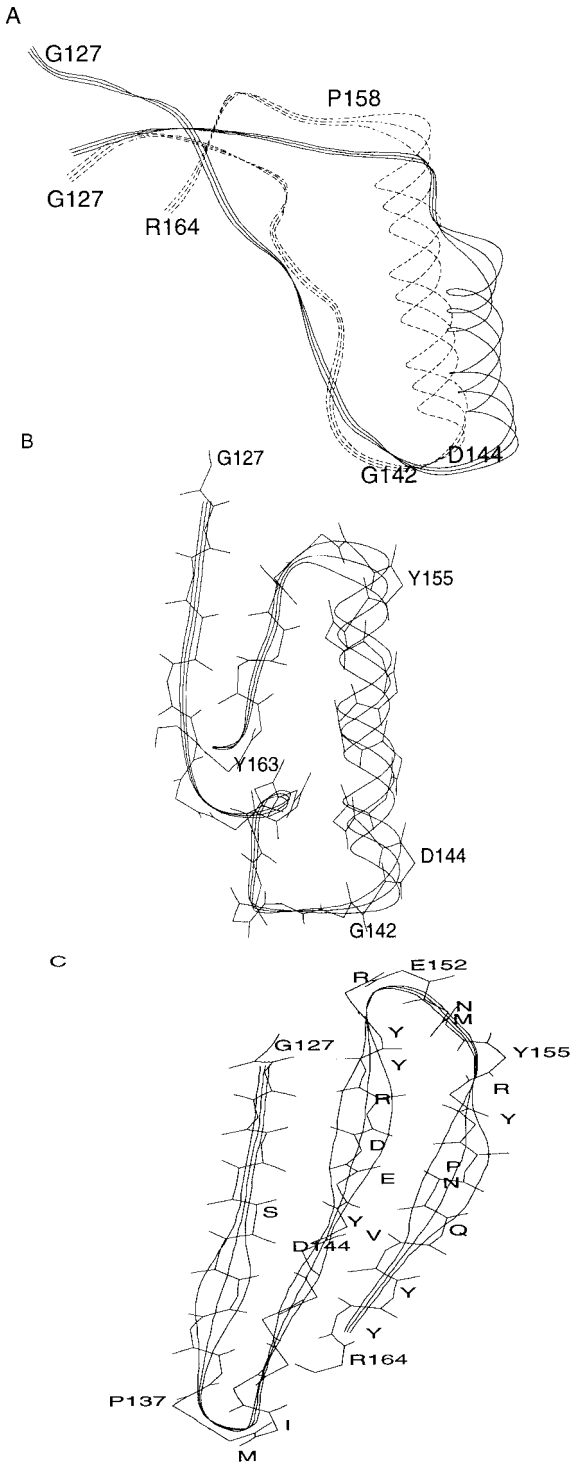

FIGURE 4 The predicted main-chain M1, M2, and M3 conformations for huPrP(127–164). (*A*) the predicted M1 conformation (*dashed line*) superposed on the full-sequence NMR solution conformation (*solid line*); (*B*) M2; (*C*) M3.

An important question is whether a small energy difference, ΔE, between the M1 and M3 conformations using the OPEP, EEF1, and AMBERGB force fields is a generic property of the PrP(127–164) sequence. To this end, we

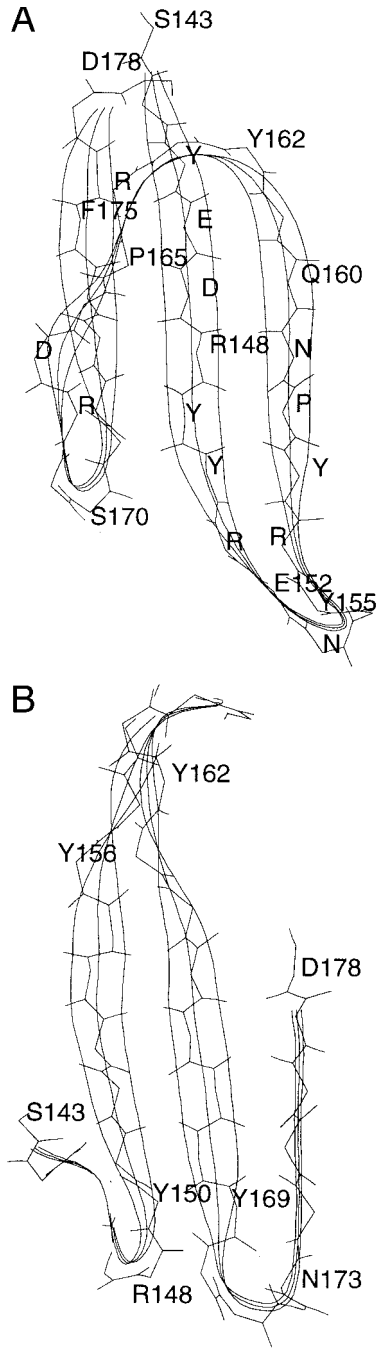

FIGURE 5 The predicted main-chain conformations for huPrP(143–178) (*A*) B1; (*B*) B2.

threaded five control sequences on the M1 and M3 conformations. The sequences are given in Fig. 1. The first control sequence is PrP(127–164) from chicken having 52% sequence identity with huPrP(127–164). The other sequences, which are not functionally related to the prion proteins, span residues 47–84 from Protein Information Resource entry T41118 (26% sequence identity with PrP), residues 101–138 from Protein Data Bank (PDB) entry 1f71, residues 30–67 from PDB entry 1lyd, and residues 40–77 from PDB entry 1mil0. The fragments from 1f71 and 1lyd were chosen because they exhibit α-helices with 10 residues (like helix H1) in their protein structures, whereas the fragment from 1mil0 adopts a β topology in its protein structure. The EEF1 energy difference between M1 and M3 is 6 kcal/mol for PrP from chicken but reaches 30, 50, 40, and 22 kcal/mol for the other sequences. These preliminary results indicate that a small ΔE is not an energetic property of any given sequence.

DISCUSSION

NMR spectroscopy has revealed that helix H1 in mPrP(143–158) switches to a β-hairpin in mPrP(142–167). The simulations yield conformational ensembles consistent with NMR data. The underlying question was to determine whether other fragments encompassing the 106–178 region have distinct conformational properties in equilibrium at pH 7.

The conclusions are based on three force fields. OPEP is a statistical energy function optimized on short peptides, whereas EEF1 and AMBERGB are two physics-based energy functions tested on large proteins. Because many force fields incorrectly rank non-native conformations as being isoenergetic or lower in free energy than native conformations, the question is whether the present conformational distribution is not an artifact of the force field that is used. Two factors suggest that the calculated minima do not correspond to metastable conformations and that the degeneracy of the ground states for PrP(106–126) and PrP(127–164) is physical. First, despite the dependence of the stability of polypeptides on pH conditions (this effect is not considered here because low pH is known to induce conformational conversion of the full PrP protein (Hornemann and Glockshuber, 1998) and CD and NMR studies of two studied fragments have been conducted at neutral pH), the OPEP-MC simulations consistently reproduce the equilibrium conformations for 31 small proteins that do and do not form ordered structures in solution. Sequences that do not form ordered (i.e., secondary) structures include a 12-residue peptide model (population of 3% of a β-hairpin structure), a 17-residue-peptide from myelin basic protein, and two isolated protein fragments, the C-helix (residues 69–87) of myohemerythrin and the helix (12–24) of chymotrypsin inhibitor 2 (Derreumaux, 1999). Ordered structures that are reproduced by OPEP-MC encompass β-hairpins, α-helical hairpins, three helix bundles (Derreumaux, 1999, 2000), and more recently, more complex topologies such as the 37-residue three-stranded anti-parallel β-sheet of a prototype WW domain from PDB entry 1e0m and the 56-residue B1 domain of protein G from PDB entry 1pgb (Derreumaux, in preparation). Second, both OPEP and EEF1 rank the expected structures first for PrP(106–126) and PrP(127–164). When the results are cross-validated with the EEF1 potential, the alternate conformations that are

collected during the OPEP-MC simulations are always less stable than the predicted conformations after energy minimization. A total of 100 decoys were considered for each protein.

Our simulations on huPrP(106–126) and huPrP(143–178) point to β topologies. The fact that the generated conformational ensembles include distinct β architectures is supported by calculations using elaborated free energy functions. PrP(106–126) appears to be in equilibrium between β-sheet structures and more disordered structures with helical units. This result is consistent with CD conformational analyses on PrP(106–126) (Salmona et al., 1999) and PrP(109–141) (Zhang et al., 1995). Because PrP(106–126) is also conformationally heterogeneous in the full PrP protein and has the propensity to make contacts with the adjacent ordered part (James et al., 1997), we believe that PrP(106–126) could initiate the topological change either spontaneously or by the point mutations P102L, P105L, and A117V. This hypothesis is supported by the recent observation that a β-sheet breaker peptide spanning PrP(115–122) partly reverses in vitro PrP^{Sc} to PrP^{C} (Soto et al., 2000), but alternative solutions combining also the amino acid 129 or interactions with PrP^{sc} (Chabry et al., 1998) cannot be excluded. The P102L mutation can be in coupling with methionine at PrP codon 129 (Young et al., 1995), whereas the codon 105 mutation is strongly correlated with codon 129 (Kitamoto et al., 1993).

On the other hand, our simulations on huPrP(127–164) show that this fragment codes for two iso-energetic topologies either with α/β structural features, as found in the NMR structure of PrP(121–231), or with β-sheet structural features. Interestingly, this β structure is characterized in the region spanning residues from 142 to 167 by a β-hairpin very similar to that found by NMR spectroscopy for mPrP(142–167) and by OPEP-MC for huPrP(143–178). Taken together, these results suggest that the region from residues 127 to 164 is likely to play a critical role in the conformational transition to PrP^{Sc} and that the β-hairpin may be preserved in the scrapie PrP^{Sc} form. Our simulations, however, cannot clarify whether a fast equilibrium exists between the M1 and M3 states. Two simulations still explore the starting M1 and M3 basins of attraction after 20,000 MC steps, but we cannot exclude the possibility that escape is feasible on a longer time scale.

Our finding of two equi-energetic conformations for the 127–164 region is consistent with NMR-structure analyses, which suggest a marginally stable 127–164 domain (James et al., 1997) and a nucleation site within this region (Riek et al., 1996). It is also in accord with a recent theoretical study that underscores the propensity for helix H1 to form stable parallel-β-sheet aggregates (Morrisey and Shakhnovich, 1999).

The existence of two iso-energetic conformations for huPrP(127–164) also provides explanations for a large body of experimental data on the full PrP protein. First, it explains why the change from neutral to acid pH conditions shifts the two-state kinetics to three-state kinetics by stabilizing a monomeric intermediate with β-sheet structure in equilibrium with the native helical state (Hornemann and Glockshuber, 1998). Such a pH variation is certainly able to increase the difference between the strength of contacts in M3 and that in M1 and therefore makes the formation of the M3 state more kinetically accessible from M1 and the unfolded state ensemble within the protein structure. Within this hypothesis, the 106–126 region is very likely to play an important role, because PrP(106–126) exhibits more β-sheet content at pH 5 (61%) than at pH 7 (40%) (Salmona et al., 1999).

Second, this conformational distribution provides a simple explanation for the position of residues contributing to the species barrier of prion transmission between mice and humans. These positions include residues 138, 143, 145, 155, and 166 (Riek et al., 1996). It is conceivable that the amino acid exchanges alter the conversion time between the M1 and M3 states in the PrP^{C}-PrP^{Sc} complex.

Third, this model allows the formation of a β-hairpin that ensures spatial proximity of the segments 142–148, 162–170 (see Fig. 5 *A*) and 214–216 of 15B3 epitope that binds selectively to PrP^{Sc}, but not to PrP^{C} (Korth et al., 1997). The last two segments were also suggested to be involved in recognition of a protein X, a hypothetical factor that might facilitate the conversion of PrP^{C} to PrP^{Sc} (Kaneko et al., 1997).

Finally, this model clarifies the location of all mutations causing prion diseases in humans (see SWISSPROT entry P04156). The M232R and P238S mutations are not considered here because they are usually removed from PrP upon addition of the glycosyl-phosphatidyl inositol anchor. These residues lie within the 127–164 region. (M129V determines the disease phenotype in patients who have a mutation at codon 178), or they bring the 127–164 region in close proximity to other segments in PrP^{C} structure. The interatomic contacts can be found from PDB entry 1AG2 using the CSU program (Sobolev et al., 1999). These mutations include A117V (contact with S1, Parchment and Essex, 2000), D178N (contact with S1, Y128 and with S2, R164), V180I (contact with V161 through V210), T183A (contact with V161), T188R or T188A or T188K (contact with R156 through F198), E196K (contact with R156), F198S (contact with R156), E200K (contact with Y149), D202N (contact with Y149 and N153), V203I (contact with Y157), R208H (contact with I139, H140 and F141), V210I (contact with V161), E211Q (contact with I139 through R208), and Q217R (contact with G131).

How then could these mutations induce the formation of PrP^{Sc} within our model? Two mechanisms can be proposed. The first mechanism involves thermodynamic destabilization of the native PrP^{C} structure in isolation and thus the native-like M1 state. Although this concept might function for particular mutations, it is not a general mechanism

underlying the formation of PrP^{Sc}. Indeed, the V180I (GSS), T183A (CJD), F198S (GSS), E200K (CJD), R208H (CJD), V210I (CJD), and Q217R (GSS) variants of mPrP(121–231) show PrP^{C}-like structural properties as deduced by CD analysis (Liemann and Glockshuber, 1999); the NMR solution structure of the E200K variant of huPrP superposes on the wild-type sequence structure (Zhang et al., 2000). The second mechanism involves reduction of the activation energy barrier between the M1 and M3 states because of PrP-PrP^{Sc} or PrP-protein X interactions.

In summary, we have shown that both PrP(106–126) and PrP(127–164) are prone to form scrapie-like β structures. In contrast to PrP(106–126) and previous model peptides studied (Derreumaux, 1999, 2000), which are predicted to be in equilibrium between their native topologies and random coil conformations, PrP(127–164) is found to code for two distinct topologies with comparable energies in isolation. Because strand S2 interacts with helices H2 and H3, the extrapolation of this energetic result to the behavior of the full PrP protein in vivo remains to be validated. Nevertheless, this conformational distribution clarifies a large body of experimental aspects and provides a simple explanation for propagating and/or triggering the PrP topological change.

I am indebted to Serguei Kozin for providing me with the NMR structure of mPrP(142–167) and for numerous discussions. I also thank Pascale Debey, Vincent Monchois, Yves-Henri Sanejouand, and the anonymous referees for helpful comments.

REFERENCES

Baskakov, I. V., C. Aagaard, I. Mehlhorn, H. Wille, D. Groth, M. A. Baldwin, S. B. Prusiner, and F. E. Cohen. 2000. Self-assembly of recombinant prion protein of 106 residues. *Biochemistry.* 39:2792–2804.

Brown, D. R., B. Schmidt, and H. A. Kretzschmar. 1996. Role of microglia and host prion protein in neurotoxicity of a prion protein fragment. *Nature.* 380:345–347.

Case, D. A., D. A. Pearlman, J. W. Caldwell, T. E. Cheatham, III, W. S. Ross, C. L. Simmerling, T. A. Darden, K. M. Merz, R. V. Stanton, A. L. Cheng, J. J. Vincent, M. Crowley, V. Tsui, R. J. Radmer, Y. Duan, J. Pitera, I. Massova, G. L. Seibel, U. C. Singh, P. K. Weiner, and P. A. Kollman. 1999. AMBER6. University of California, San Francisco.

Chabry, J., B. Caughey, and b. Chesobro. 1998. Specific inhibition of in vitro formation of protein-resistant prion protein by synthetic peptides *J. Biol. Chem.* 273:13203–13207.

Derreumaux, P. 1999. From polypeptide sequences to structures using Monte Carlo simulations and an optimized potential *J. Chem. Phys.* 111:2301–2310.

Derreumaux, P. 2000. Generating ensemble averages for small proteins from extended conformations by Monte Carlo simulations *Phys. Rev. Lett.* 85:206–209.

Downing, D. T., and N. D. Lazo. 1999. Molecular modelling indicates that the pathological conformations of prions might be β-helical *Biochem. J.* 343:453–460.

Duan, Y., and P. Kollman. 1998. Pathways to a protein folding intermediate observed in a 1-microsecond simulation in aqueous solution. *Science.* 282:740–744.

Ettaiche, M., R. Pichot, J. P. Vincent, and J. Chabry. 2000. In vivo cytotoxicity of the prion protein fragment 106–126. *J. Biol. Chem.* 275:36487–36490.

Ghetti, B., P. Piccardo, M. G. Spillantini, Y. Ichimiya, M. Porro, F. Perini, T. Kitamoto, J. Tateishi, C. Seiler, B. Frangione, O. Bugiani, G. Giaccone, F. Prelli, M. Goedert, S. R. Dlouhy, and F. Tagliavini. 1996. Vascular variant of prion protein cerebral amyloidosis with tau-positive neurofibrillary tangles: the phenotype of the stop codon 145 mutation in PRNP. *Proc. Natl. Acad. Sci. U.S.A.* 93:744–748.

Holm, L., and C. Sander. 1992. Fast and simple Monte Carlo algorithm for side chain optimization in proteins. *Proteins.* 14:213–223.

Hornemann, S., and R. Glockshuber. 1998. A scrapie-like unfolding intermediate of the prion protein domain PrP(121–231) induced by acidic pH. *Proc. Natl. Acad. Sci. U.S.A.* 95:6010–6014.

Huang, Z., S. B. Prusiner, and F. E. Cohen. 1996. Scrapie prions: a three-dimensional model of an infectious fragment. *Fold. Design.* 1:13–19.

James, T. L., H. Liu, N. B. Ulyanov, S. Farr-Jones, H. Zhang, D. G. Donne, K. Kaneko, D. Groth, I. Mehlhorn, S. B. Prusiner, and F. E. Cohen. 1997. Solution structure of a 142-residue recombinant prion protein corresponding to the infectious fragment of the scrapie isoform. *Proc. Natl. Acad. Sci. U.S.A.* 94:10086–10091.

Jarrett, J. T., and P. T. Lansbury, Jr. 1993. Seeding one dimensional crystallization of amyloid: a pathogenic mechanism in Alzheimer's disease and scrapie? *Cell.* 73:1055–1058.

Kaneko, K., L. Zulianello, M. Scott, C. M. Cooper, A. C. Wallace, T. L. James, F. E. Cohen, and S. B. Prusiner. 1997. Evidence for protein X binding to a discontinuous epitope on the cellular prion protein during scrapie prion propagation *Proc. Natl. Acad. Sci. U.S.A.* 94:10069–10074.

Kitamoto, T., M. Ohta, K. Doh-ura, S. Hitoshi, Y. Terao, and J. Tateishi. 1993. Novel missense variants of prion protein in Creutzfeldt-Jacob disease or Gerstmann-Straussler syndrome. *Biochem. Biophys. Res. Commun.* 191:709–714.

Koehl, P., and M. Delarue. 1994. Application of a self-consistent mean field theory to predict protein side-chains conformation and estimate their conformational entropy. *J. Mol. Biol.* 239:249–275.

Korth, C., B. Stierli, P. Streit, M. Moser, O. Schaller, R. Fischer, W. Schulz-Schaeffer, H. Kretzschmar, A. Raeber, U. Braun, F. Ehrensperger, S. Hornemann, R. Glockshuber, R. Riek, M. Billeter, K. Wuthrich, and B. Oesch. 1997. Prion(PrP^{Sc})-specific epitope defined by a monoclonal antibody. *Nature.* 390:74–77.

Lazaridis, T., and M. Karplus. 1998. Discrimination of the native from misfolded protein models with an energy function including implicit solvation. *J. Mol. Biol.* 288:477–487.

Liemann, S., and R. Glockshuber. 1999. Influence of amino acid substitutions related to inherited human prion diseases on the thermodynamic stability of the cellular prion protein. *Biochemistry.* 38:3258–3267.

Liu, A., R. Riek, R. Zahn, S. Hornemann, R. Glockshuber, and K. Wuthrich. 1999. Peptides and proteins in neurodegenerative disease: helix propensity of a polypeptide containing helix 1 of the mouse prion protein studied by NMR and CD spectroscopy. *Biopolymers.* 51:145–152.

Maiti, N. R., and W. K. Surewicz. 2001. The role of disulfide bridge in the folding and stability of the recombinant human prion protein. *J. Biol. Chem.* 276:2427–2431.

Metropolis, N. S., A. W. Rosenbluth, M. N. Rosenbluth, A. H. Teller, and E. Teller. 1953. Equation of state calculations by fast computing machines *J. Chem. Phys.* 21:1087–1092.

Morrisey, M. P., and E. I. Shakhnovich. 1999. Evidence for the role of PrP^{C} helix 1 in the hydrophilic seeding of prion aggregates. *Proc. Natl. Acad. Sci. U.S.A.* 96:11293–11298.

Parchment, O. G., and J. W. Essex. 2000. Molecular dynamics of mouse and Syrian hamster PrP: implications for activity. *Proteins.* 38:327–340.

Peretz, D., R. A. Williamson, Y. Matsunaga, H. Serban, C. Pinilla, R. B. Bastidas, R. Rozenshteyn, T. L. James, R. A. Houghten, F. E. Cohen, S. B. Prusiner, and D. R. Burton. 1997. A conformational transition at the N terminus of the prion protein features in formation of the scrapie isoform. *J. Mol. Biol.* 273:614–22.

Prusiner, S. B. 1997. Prion diseases and the BSE crisis. *Science.* 278: 245–251.

Riek, R., S. Hornemann, G. Wider, M. Billeter, R. Glockshuber, and K. Wuthrich. 1996. NMR structure of the mouse prion protein domain PrP(121–231). *Nature.* 382:180–182.

Salmona, M., P. Malesani, L. De Gioia, S. Gorla, M. Bruschi, A. Molinari, F. Della Vedova, B. Pedrotti, M. A. Marrari, T. Awan, O. Bugiani, G. Forlomi, and F. Tagliavini. 1999. Molecular determinants of the physicochemical properties of a critical prion protein region comprising residues 106–126. *Biochem. J.* 342:207–214.

Sharman, G. J., N. Kenward, H. E. Williams, M. Landon, R. J. Mayer, and M. S. Searle. 1998. Prion protein fragments spanning helix 1 and both strands of beta sheet (residues 125–170) show evidence for predominantly helical propensity by CD and NMR. *Fold. Design.* 3:313–320.

Sobolev, V., A. Sorokine, J. Prilusky, E. E. Abola, and M. Edelman. 1999. Automated analysis of interatomic contacts in proteins. *Bioinformatics.* 15:327–332.

Soto, C., R. J. Kascsak, G. P. Saborio, P. Aucouturier, T. Wisniewski, F. Prelli, R. Kascsak, E. Mendez, D. A. Harris, J. Ironside, F. Tagliavini, R. I. Carp, and B. Frangione. 2000. Reversion of prion protein conformational changes by synthetic β-sheet breaker peptides. *Lancet.* 355: 192–197.

Sparrer, H. E., A. Santoso, F. C. Szoka, Jr., and J. S. Weissman. 2000. Evidence for the prion hypothesis: induction of the yeast [psi$^+$] factor by in vitro-converted sup35 protein. *Science.* 289:595–599.

Supattapone, S., P. Bosque, T. Muramoto, H. Wille, C. Aagaard, D. Peretz, H. O. Nguyen, C. Heinrich, M. Torchia, J. Safar, F. E. Cohen, S. J. DeArmond, S. B. Prusiner, and M. Scott. 1999. Prion protein of 106 residues creates an artificial transmission barrier for prion replication in transgenic mice. *Cell.* 96:869–878.

Young, K., C. K. Jones, P. Piccardo, A. Lazzarini, L. I. Golbe, T. R. Zimmerman, Jr., D. W. Dickson, D. C. McLachlan, P. St. George-Hyslop, and A. Lennox. 1995. Gerstmann-Straussler-Scheinker disease with mutation at codon 102 and methionine at codon 129 of PRNP in previously unreported patients. *Neurology.* 45:1127–34.

Zahn, R., A. Liu, T. Luhrs, R. Riek, C. von Schroetter, F. Lopez Garcia, M. Billeter, L. Calzolai, G. Wider, and K. Wuthrick. 2000. NMR solution structure of the human prion protein. *Proc. Natl. Acad. Sci. U.S.A.* 97:145–150.

Zhang, H., K. Kaneko, J. T. Nguyen, T. L. Livshits, M. A. Baldwin, F. E. Cohen, T. L. James, and S. B. Prusiner. 1995. Conformational transitions in peptides containing two putative α-helices of the prion protein. *J. Mol. Biol.* 250:514–526.

Zhang, Y., W. Swietnicki, M. G. Zagorski, W. K. Surewicz, and F. D. Sonnichsen. 2000. Solution structure of the E200K variant of human prion protein *J. Biol. Chem.* 275:33650–33654.